Structural and dynamical fingerprints of the anomalous dielectric properties of water under confinement

Iman Ahmadabadi,[1] Ali Esfandiar,[1] Ali Hassanali,[2,*] and Mohammad Reza Ejtehadi[1,†]
[1]*Department of Physics, Sharif University of Technology, Tehran 14588-89694, Iran*
[2]*The Abdus Salam International Centre for Theoretical Physics, Strada Costiera 11, 34151 Trieste, Italy*

(Received 28 September 2020; accepted 8 February 2021; published 26 February 2021)

There is a long-standing question about the molecular configuration of interfacial water molecules in the proximity of solid surfaces, particularly carbon atoms, which plays a crucial role in electrochemistry and biology. In this study, the dielectric, structural, and dynamical properties of confined water placed between two parallel graphene walls at different interdistances from the angstrom scale to a few tens of nanometer have been investigated using molecular dynamics. For the dielectric properties of water, we show that the dielectric constant of the perpendicular component of water drastically decreases under sub-2-nm spatial confinement. The dielectric constant data obtained through linear response and fluctuation-dissipation theory are consistent with recent reported experimental results [L. Fumagalli *et al.*, Science **360**, 1339 (2018)]. By determining the charge density as well as fluctuations in the number of atoms, we provide a molecular rationale for the behavior of the perpendicular dielectric response function. We also interpret the behavior of the dielectric response in terms of the presence of dangling O-H bonds of water. By examining the residence time and lateral diffusion constant of water under confinement, we reveal that the water molecules tend to keep their hydrogen bond networks at the interface of water-graphene. We also found consistency between lateral diffusion and the z-component of variance in the center of mass of the system as a function of confinement.

DOI: 10.1103/PhysRevMaterials.5.024008

I. INTRODUCTION

It is well known that the behavior of interfacial water governs both its rheology and its physical properties in a wide range of phenomena in nature [1–3]. To understand the interaction and structure of water in contact with solid surfaces, various experimental and theoretical efforts have been applied in the literature. One of the most studied systems in this regard is the behavior of water near hydrophobic interfaces, specifically near graphene [4–20]. Due to the obvious general relevance, the graphene/water interface has been an attractive system to simulate and study the dynamics of water. This has numerous practical implications. In particular, the presence of water in ultranarrow slits and membranes in biology and porous electrodes in electrochemistry makes the graphene-water system the subject of numerous studies [4–21].

It is well appreciated that water near interfaces is perturbed both in terms of its structural and dynamical properties. In the case of hydrophilic surfaces, water forms interactions with the interface and subsequently leads to a slow-down in the water dynamics by a factor of about 4–7. On the other hand, near hydrophobic interfaces, there is a length scale dependence to the dewetting behavior [1]. As one brings two interfaces close to each other, we enter the regime of confined water. There have been many experimental and theoretical studies investigating how both thermodynamic and dynamical properties of water change under confinement [22–41]. It is beyond the scope of the current paper to review all this literature. However, we note that there are several interesting thermodynamic and dynamic anomalies that have been observed when water is placed in confined conditions. In this work, we focus on how dielectric properties of water change when sandwiched between two graphene sheets.

In previous reports, it was shown that the graphene-water interface induces an orientational polarization of water in close proximity to the surface. This orientational configuration directly affects other properties of water at the interface, such as the dielectric response [22–38]. However, there have been relatively fewer studies investigating how the dielectric constant of water changes under confinement using both experiments and simulations.

Recently, Fumagalli and co-workers [42] have used atomic force microscopy (AFM) methods to study the molecular polarization of water molecules by applying ac voltage between the AFM tip and the surface of graphite. The results of this experiment confirm the suppression of the polarizability of confined water within nanocapillaries. Because of the possible arrangement of interfacial molecules and bulk water, there are different charge distributions in these two regimes resulting in a surface capacitance. This feature has been used in order to measure the perpendicular dielectric constant of water under various confinements. It is known that the perpendicular component of the dielectric constant is related to the zeta potential and surface capacitance [43,44].

One of the features of water that makes it unique is its large polarizability. This gives bulk water its large static dielectric constant. Several previous studies have examined

*ahassana@ictp.it
†ejtehadi@sharif.edu

how the dielectric properties of water change under confinement [31,34]. Water confined between two graphene walls exhibits anomalous behavior because of the suppression of polarization. This results in drastically low values of perpendicular dielectric response [35]. In addition, it is worth noting that the structuring of water near interfaces in general is thought to be the dominant factor in controlling the position-dependent dielectric permittivity of the system [36].

The motivation for the calculations reported in this work come from some recent experiments measuring the anomalous dielectric properties of water under confinement [42]. Specifically, in this work by using a combination of a height-tunable method for two-dimensional capillaries made by atomically flat walls, and scanning dielectric microscopy through electrostatic force detection by means of AFM, the molecular polarization of confined water has been measured. In this experiment, by applying a low-frequency ac voltage between the AFM tip and the bottom of the graphite electrode, the tip-substrate can be identified as a first derivative of local capacitance $\frac{dC}{dz}$ in a vertical direction. The measured data indicated that epsilon and consequently the polarizability of the confined water is suppressed intensely in nanochannels with less than 10 nm height.

In this work, the dielectric behavior of water between two graphene layers has been determined via molecular dynamics (MD) simulations. We show that the effective perpendicular dielectric constant of water reduces substantially when the distance between two graphene layers decreases below ∼2 nm, in complete agreement with recent experimental results [42]. We have also investigated the local value of the dielectric permittivity of water as a function of different extents of confinement, and we find that it reduces to near vacuum permittivity for regions close to the surface. This has also been the subject of some recent simulation work, although the molecular signatures in terms of both static and dynamical properties have not been fully investigated [36–38]. To understand better the origins of the changes of the dielectric properties under confinement, we determine some structural and dynamical properties of water. Specifically, we compute the residence times and diffusion constant of water as a function of confinement. We find that water molecules at the early layers from the surface tend to keep their location for a longer amount of time than when they are in the bulk regions. The residence time as well as diffusion constant results are consistent with the presence of a layer of structured water near the surface of graphene.

The paper is organized in the following manner. We begin in Sec. II by introducing the computational method we have used in this work. Then in Sec. III A, we present the results on the dielectric properties of confined water between graphene walls as a function of distance from the surface as well as the effective values of the dielectric constant for various thicknesses of water slabs. Additionally, we relate the permittivity results to the other properties of water, such as its hydrogen bond network. In Sec. III B, we present the residence time as well as the diffusion constant as a dynamical analysis in order to make a coherent picture of the structure and dynamics in the surface of water under confined conditions.

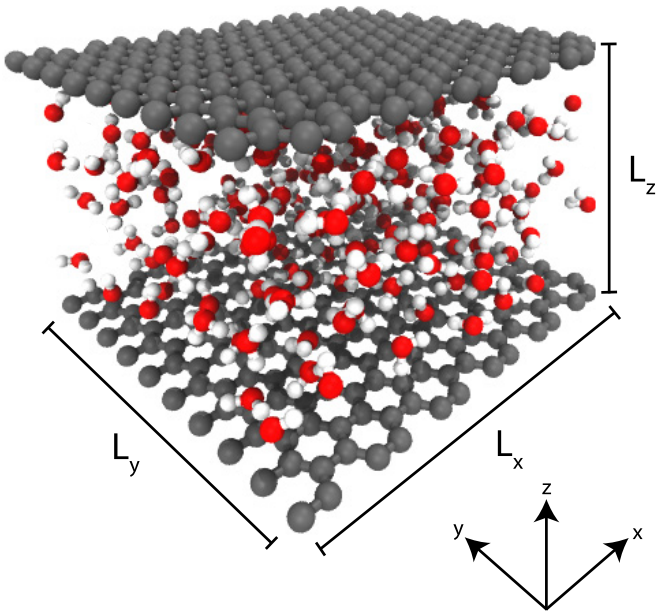

FIG. 1. Water molecules under two-dimensional slits and graphene walls. Gray balls represent carbon atoms, red balls denote oxygen, and white balls denote hydrogen. This figure is not scaled in the x and y directions according to real system cell parameters.

II. COMPUTATIONAL METHODS

We use the SPC/E model of water [45] for our simulations, which has been shown to reproduce the dielectric properties of water rather well. The density of water is 1 g/mL in slab geometries, ranging from 534 (a monolayer of water) up to 184 206 molecules for nearly bulk conditions, which span different layered structures of confined water molecules. In version 5.2 of the GROMACS package [46], we have used the force field proposed by Werder *et al.* [30] for water-carbon interactions. This potential has previously been validated by reproducing the contact angle of water near graphene [30]. The temperature of the system for all simulations is 298.15 K using the Nose-Hoover thermostat [47,48]. The graphene walls consist of carbon atoms with zero charge, and they are completely flat and parallel to each other. Periodic boundary conditions were applied in all three directions. The box dimensions are 6.63 nm × 6.95 nm × (L_z + 2 nm), where L_z is the distance between graphene walls between which the water is placed.

Simulations were run for 0.2 μs for each distance below 100 Å and 10 ns for the thicker height of two-dimensional slits, using a 1 fs time step. The truncated radius for the Lennard-Jones interactions is $r = 1.4$ nm using the Verlet scheme, and the particle mesh Ewald (PME) summation [49] is used for treating the electrostatic interactions. A schematic view of the graphene-water channel system is shown in Fig. 1.

III. RESULTS

A. Dielectric response

In this section, we present our analysis of the perpendicular dielectric response of water and how it changes as a function of distance from the surface. The change in dielectric

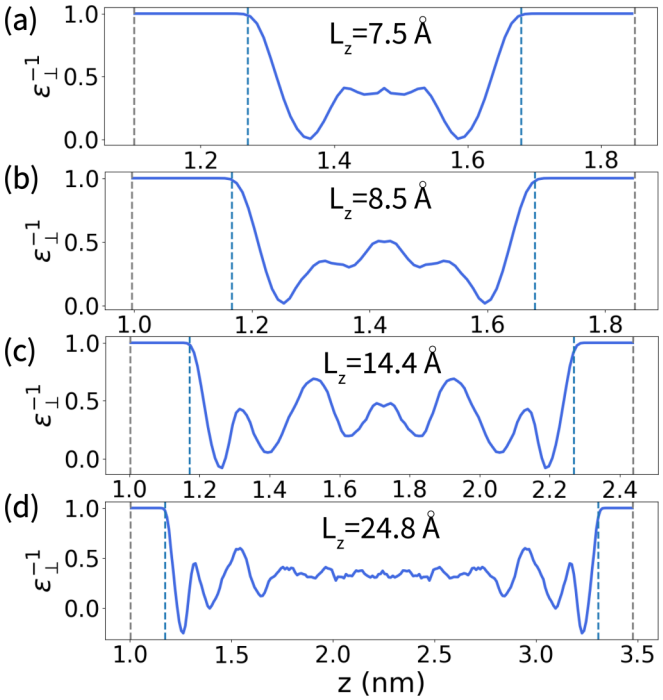

FIG. 2. Inverse of the perpendicular component of the dielectric constant for different wall distances as a function of height z. Gray and blue vertical dashed lines indicate the surfaces of graphene and water, respectively. Different thicknesses of water slabs are (a) $L_z = 7.5$ Å, (b) $L_z = 8.5$ Å, (c) $L_z = 14.4$ Å, and (d) $L_z = 24.8$ Å.

displacement field is related linearly to the change of the electric field in the linear-response regime. In Appendix A, the linear response theory of a dielectric constant has been reviewed [25,34,35,39,40]. The most relevant equation for the dielectric response across the graphene-water channel that is used in our simulations is the following:

$$\varepsilon_{\perp}^{-1}(z) = 1 - \frac{\Delta m_{\perp}(z)}{\varepsilon_0 k_B T + C_{\perp}/V}, \tag{1}$$

where $\Delta m_{\perp}(z)$ is the polarization along the z direction, and $C_{\perp}$ is the polarization correlation function integrated over height z as calculated in Appendix A. V is the volume of the water slab. T, k_B, and ε_0 are the temperature, Boltzmann's constant, and vacuum permittivity, respectively.

The calculated results for the inverse of the perpendicular component of dielectric constant $\varepsilon_{\perp}$ as a function of the interdistance of graphene walls for a different water slab are presented in Fig. 2. In close proximity to the graphene surfaces, the dielectric function of water in the perpendicular direction is significantly reduced, consistent with previous studies [25,30,34,41,50–53]. Interestingly, under confinement there are some marked oscillations in the perpendicular component of the dielectric constant that acquire even negative values near the interface. Generally, the negative values are due to the external field overscreening of interfacial water molecules. Therefore, water dipolar high polarization induces an inverse electric field, resulting in negative values of the dielectric function [31–34]. We will discuss further these oscillations and relate them to other properties of water in subsequent sections.

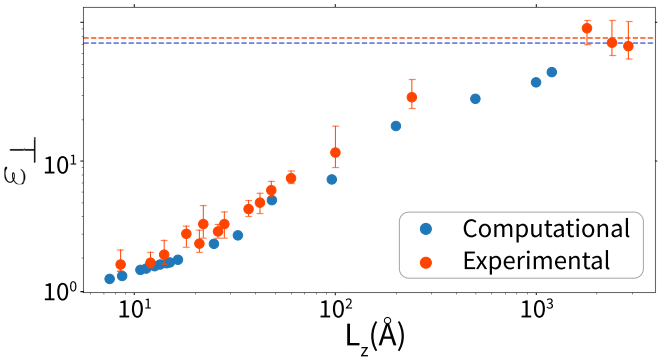

FIG. 3. Computational (blue data) and experimental (red data) perpendicular component of the dielectric constant for different distances of graphene walls. Corresponding dashed lines indicate the bulk values of the SPC/E water model (∼71) and pure water. The error bars of computational data are small, staying inside of each data circle.

To relate the perpendicular component of the dielectric constant shown earlier to the experimentally measured *effective* dielectric constant [42], some preliminary steps are needed. Integrating $\varepsilon_{\perp}^{-1}$ in Eq. (1) over the channel results in Eq. (2), which has two unknowns $L_{\perp}^{\text{eff}}$ and $\varepsilon_{\perp}^{\text{eff}}$. Since we have two of these unknown parameters, we decided to determine the value of $L_{\perp}^{\text{eff}}$ by first using the value of $\varepsilon_{\perp}^{\text{eff}}$ for the smallest confined system, and using that to reverse engineer the value of $L_{\perp}^{\text{eff}}$. Specifically, we used the initial value $\varepsilon_{\perp}^{\text{eff}} = 1.4$ for $L_z = 7.5$ Å experimentally measured as the narrowest interdistance between graphene walls, and we obtained $L_{\text{eff}} - L_z = 0.94$ Å [40]. Assuming that the difference between $L_{\perp}^{\text{eff}}$ and L_z remains constant for higher L_z, and therefore by knowing L_{eff}, we can determine the $\varepsilon_{\perp}^{\text{eff}}$ for all L_z. These results are shown in Fig. 3. For clarity, the reader is reminded that in Eq. (2), L_w corresponds to the length of the region where the density of water is nonzero (the distance between two blue-dashed lines in Fig. 9 in Appendix B),

$$\int_{-L_w/2}^{L_w/2} \varepsilon_{\perp}^{-1}(z)dz = L_{\perp}^{\text{eff}}\left(\frac{1}{\varepsilon_{\perp}^{\text{eff}}} - 1\right) + L_w. \tag{2}$$

Using Eq. (2), L_{eff} can be calculated from L_w. Assuming the same values for the difference between acquired $L_{\perp}^{\text{eff}}$ and L_w for other confinements, we can calculate $\varepsilon_{\perp}^{\text{eff}}$ for all other water slab thicknesses. As we can observe from Fig. 3, the perpendicular component is very low and close to 1.4 in all slab thicknesses less than ∼15 Å, and then it increases to bulk values gradually. The trend of our calculated results is in good agreement with recently reported experimental data [42]. Interestingly, the length scale required for the dielectric constant to converge to the bulk value is quite large (over 1000 Å), and it is much longer than that needed to converge radial and orientational correlations.

We next turn to examining the evolution of the hydrogen bond network in order to understand why the dielectric properties change under confinement. We begin first by examining how the orientation of water changes near the graphene layer. To analyze the orientation of hydrogen bonds as a function of z in the slab of water, we calculated the time-averaged z component of dipole moments for water molecules. The maximum

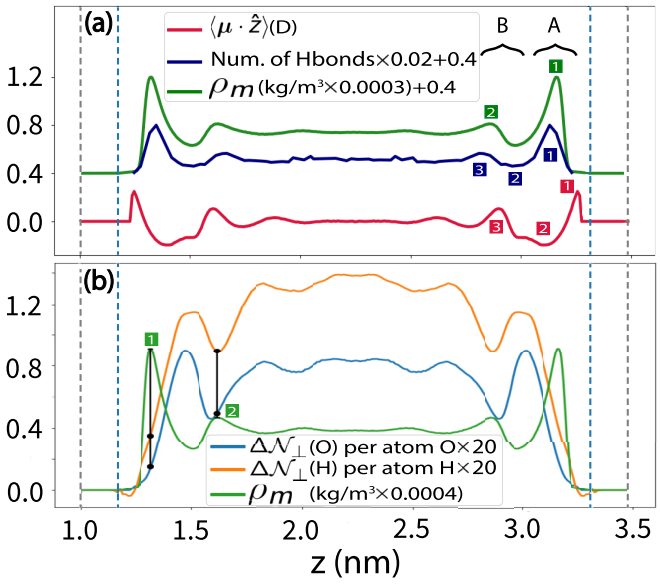

FIG. 4. (a) The time-averaged z component of dipole moments of water molecules as a function of height z. Regions A and B correspond to the first and second layer estimated by the density of particles (blue curve), respectively. Additionally, the green curve presents the number of H-bonds. The slab thickness is $L_z = 24.8$ Å. The particle density and number of hydrogen bonds have been multiplied by 0.0003 and $\frac{1}{50}$, respectively, as a rescaling for a better display. (b) The fluctuations in the number of hydrogen and oxygen per atom of each type as a function of height z for thickness $L_z = 24.8$ Å. The diagrams of $\Delta\mathcal{N}_\perp(H)$, $\Delta\mathcal{N}_\perp(O)$, and density of particles have been multiplied by 20, 20, and $\frac{1}{2500}$.

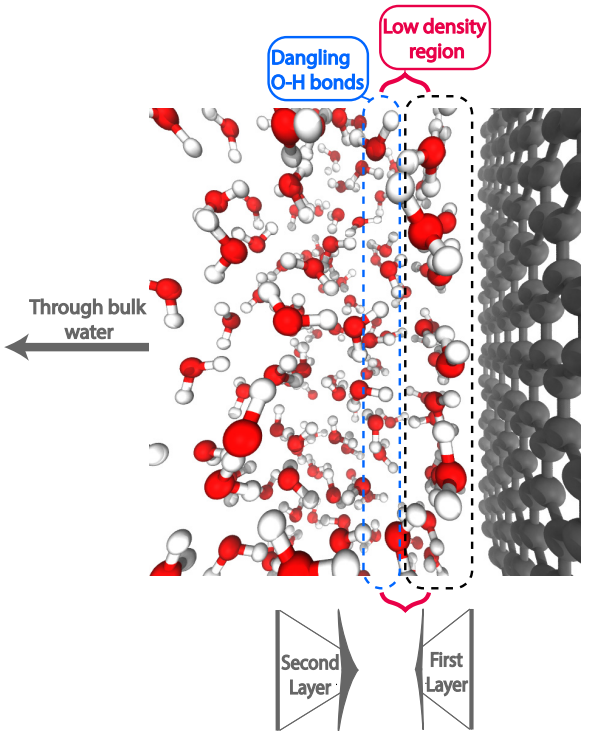

FIG. 5. Schematic figure for a few layers of water near the interface of water-graphene.

1-red in Fig. 4(a) adjacent to the graphene walls demonstrates the tendency of the O-H bonds to interact with carbon atoms, and as a result, to be directed into the graphene sheets. In the first interfacial layer shown by region A, due to the hydrogen bond network, most of the water molecules spend time in a planar configuration (see also Fig. 5). However, there is a small tilting from the x-y plane by $\sim 10^\circ$ corresponding to the minimum 2-red in Fig. 4(a). This can be considered as the criterion of the planar hydrogen bond for water molecules at the interface [36].

Since the sign of the averaged dipole moment in the minimum 2-red is opposite to that of the maximum 1-red, we conclude that the deviation from the planar configuration at the bottom of the first layer is directed into the low-density region below the first layer. The nonzero value of the dipole moment in the z direction in the second layer, corresponding to section B (maximum 3-red and 2-green), is consistent with the dangling O-H bonds as discussed in the previous sections. As is shown in region B in Fig. 4(a), the z-component dipole moment in the maximum 3-red has the same sign as the hydrogen bonds adjacent to the graphene walls, meaning that dangling O-H bonds are directed into the low-density region between the first and second layers of interfacial water (see also Fig. 5). To further assert this argument, the number of H-bonds have been computed as a function of height z [Fig. 4(a)]. The hydrogen bond criterion was determined by the standard Luzar and Chandler recipe [54]. The maximum 1-green indicates the high number of H-bonds in the first layer, as we expect from the H-bond network. The minimum 2-blue in Fig. 4(a) corresponds to the lack of H-bonds in the low-density region and early parts of the second layer. The minimum 2-blue has entered into the second layer (maximum 2-green), which indicates that water molecules at the early parts of the second layer create fewer H-bonds in comparison to the deeper parts of water, which indicates the presence of dangling O-H bonds.

The preceding analysis does not explain the changes in the fluctuations of the various degrees of freedom involving the solvent as it approaches the graphene layers. Toward this end, we computed the Fano factors associated with the oxygen and hydrogen atoms individually as a function of position along the z direction [see Fig. 4(b)]. The Fano factor is defined as

$$\Delta\mathcal{N}_{\perp,X}(z) \equiv \frac{\langle N_X^2(z)\rangle - \langle N_X(z)\rangle^2}{\langle N_X(z)\rangle}. \tag{3}$$

Note that $\langle\cdots\rangle$ is the time average over the whole trajectory, and $N_X(z)$ is the number of atoms X (oxygen or hydrogen) at height z. It is worth mentioning that several previous studies have shown that the Fano factor can be used to probe the local compressibility of water [55]. As expected, the lighter mass of hydrogen is characterized by larger Fano factors. In the first layer [maximum 1 in Fig. 4(b)], the ratio of fluctuations in the number of hydrogen atoms to fluctuations in the number of oxygen atoms is $\frac{\Delta\mathcal{N}_{\perp,\mathrm{H}}}{\Delta\mathcal{N}_{\perp,\mathrm{O}}} \simeq \frac{0.35}{0.15} = 2.33$, while this ratio for the second layer [maximum 2 in Fig. 4(b)] is $\frac{\Delta\mathcal{N}_{\perp,\mathrm{H}}}{\Delta\mathcal{N}_{\perp,\mathrm{O}}} \simeq \frac{0.9}{0.5} = 1.8$. This indicates that although fluctuations in the number of both hydrogen and oxygen atoms in the first layer are smaller than those in the second layer and the rest of water, the ratio of fluctuations for the first layer is larger than that for the remaining part of water. Consistent with the results

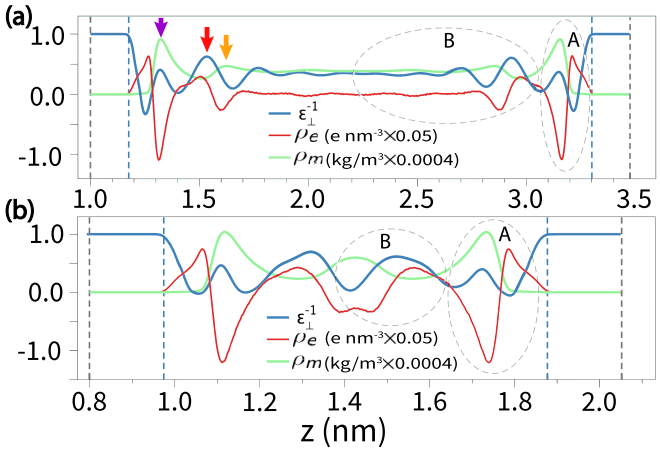

FIG. 6. (a) The purple marker and $\varepsilon_\perp^{-1}$ maximum determine the restriction of water molecules in order to rotate out of the x-y plane, causing a very low dielectric constant. The red area is compatible with the low-density region between the first and second layer of the water molecules. The orange zone shows the presence of dangling OH bonds, leading to higher values for $\varepsilon_\perp$. The slab thickness is $L_z = 24.8$ Å. (b) Inverse of the perpendicular component of the dielectric constant vs the density of charges as well as the density of particles. Region A shows the opposite behavior of $\varepsilon_\perp^{-1}$ and the density of charges (ρ_e). Region B indicates the consonant trend between $\varepsilon_\perp^{-1}$ and ρ_e. The water thickness is $L_z = 12.5$ Å. The diagrams for ρ_e and ρ_m have been scaled up via dividing the values by 20 and 2500, respectively.

presented in the previous sections, in the first layer, hydrogen atoms can rotate around oxygens (as mostly fixed points) in order to align the water molecule along the direction of the applied field. However, this behavior is reversed in bulk water, where the whole water molecule tends to rotate around a point on the dipole vector.

The molecular signatures of water's hydrogen bond network near the graphene surface have profound implications on the dielectric constant and how it evolves as a function of distance from the graphene surface. Consistent with recent studies [36], the most energetically favorable and therefore most probable orientations of water molecules close to graphene tend to have their dipole oriented parallel to the solid surface, creating a network of H-bonds at the graphene-water interface. This hydrogen-bond network cannot be aligned along the perpendicular directed external field for the response, and as a result, an overscreening layer is created for the external electric field.

As can be seen from Fig. 2, there are a set of maxima and minima close to the interface of water. The first maximum in $\varepsilon_\perp^{-1}(z)$ is related to the first layer of water [the area indicated by purple in Fig. 6(a)]. This maximum can be assigned to a network of H-bonds in water molecules mostly parallel to the graphene sheets. This layer is responsible for screening effects, and interrupting this network via an external field is energetically unfavorable. Another consequence of this screening effect is the diverging or more intensively the negative values for $\varepsilon_\perp(z)$ (the first minima at the interfaces in Figs. 2 and 6 for $\varepsilon_\perp^{-1}$) close to the surface of water.

To dig deeper into the origins of the oscillations of the dielectric constant, we investigated the coupling between the mass and charge density of particles as shown in Fig. 9. We begin by examining the evolution in the mass density. Due to the separation of the first layer with the rest of the water molecules, there is a low-density region as thin as 2 Å between the first and second layers, which is mostly filled with hydrogen atoms rather than oxygen ones. This region is shown schematically in Fig. 5 in the yellow region. Because of the lack of water molecules in this region for the response to the external electric field, $\varepsilon_\perp^{-1}$ reaches its maximum value in comparison to the other maxima in the graph [red area in Fig. 6(a)]. It can be concluded that water molecules in the second layer cannot make enough H-bonds with the first layer. As a result, they are left with dangling OH bonds as shown in Fig. 5. Since these dangling OH bonds have more freedom to rotate, especially out of the x-y plane, they can respond to the external field stronger than OH bonds in the first layer, which are involved in a robust hydrogen-bond network. This higher response leads to higher values of $\varepsilon_\perp(z)$. A few more tenths of an angstrom further into the bulk after the second maximum in the density of particles, $\varepsilon_\perp$ reaches a maximum. This is in agreement with the existence of dangling OH bonds in the second layer [orange area in Fig. 6(a) and blue dashed rectangle in Fig. 5]. Note that this minimum in $\varepsilon_\perp^{-1}$ occurs for all thicknesses of the water slab considered in our work and thus appears to be a generic phenomenon.

In addition to the mass density, there are also some interesting features involving the coupling between the charge density and the dielectric constant. In the vicinity of the graphene sheets, the changes of the charge density and the $\varepsilon_\perp^{-1}$ are anticorrelated, while in the bulk they are correlated (see Fig. 6, marked as A and B, respectively). This indicates that in the first layer, oxygen atoms can hardly participate in the dielectric response due to their heavier mass and rigidity in movement through the hydrogen-bond network, as explained earlier.

A simple picture of the configuration is that each oxygen atom can host two H-bonds in addition to the two covalent bonds with the hydrogen atoms within the water molecule. Thus, oxygen atoms are involved in the creation of four H-bonds. In contrast, hydrogen atoms can only be involved between two oxygen atoms in an H-bond. Hence, out-of-plane movement of oxygen atoms can destruct the H-bond network more effectively than hydrogen's out-of-plane rotation. Therefore, the rotation of hydrogen toward the graphene layer around oxygen atoms is the dominant response mechanism to the external field in region A. In contrast, in the second layer as well as the rest of the water, the changes in the charge density and $\varepsilon_\perp^{-1}$ are consonant. This reflects the fact that the rotation of both oxygen and hydrogen atoms together around the center of mass of the water molecule contributes to the response mechanism. Due to the absence of an H-bond network here, this rotation can occur without the energetically unfavorable disturbing of any H-bond network. Therefore, since the center of mass of a water molecule is closer to the oxygen atom than the hydrogen atom, the response to the external field becomes consonant with the presence of oxygen atoms (Fig. 6).

B. Dynamical properties

In the previous section, we have focused on identifying static molecular signatures of the hydrogen-bond network

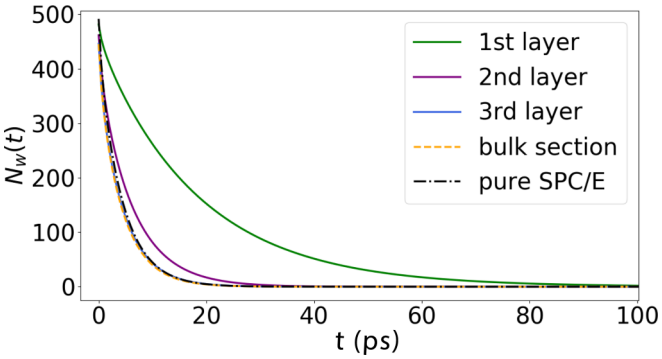

FIG. 7. Residence time correlation function of water molecules between graphene walls for $L_z = 24.8$ Å. The residence time is obtained for early layers of each system, indicating that the first layer (green line) has the longest residence time, and then the second layer (purple line) is the layer with the highest survival time. The third layer (blue line) and the bulk segments (orange dashed line) of the confined channel have mostly the same residence time with pure SPC/E water (black dashed-dotted lines) without confinement.

in order to correlate them with the behavior in the dielectric constant. We move next to understanding and searching for whether these features are also reflected in the dynamic quantities. Specifically, we focus on two dynamical properties, namely the residence time and the diffusivity. We have followed the residence time of water molecules for different layers of confined water. The definition of the residence time correlation function is given by the following equation, as was done in numerous previous studies [56–58]:

$$N_w(t) = \frac{1}{N_t} \sum_{n=1}^{N_t} \sum^{i} P_i(t_n, t), \tag{4}$$

in which the conditional probability $P_i(t_n, t)$ is 1 if the ith water molecule remains in the selected region in t_n and $t_n + t$ time interval, otherwise it is zero. N_t is the number of time-frames with length t in which we calculate the survival probabilities. Here, we have estimated different selected layers of water based on the density profiles. Typically, the first layer of water calculated from one of the graphene sheets relates to the first maximum of the particle density diagram. We have considered ∼3 Å as the thickness of a single layer of water, in which the maximum value of the particle density is in the center of the selected region for each layer. As a result of planar hydrogen-bond networks, we expect that the layered structure of water mostly exists at the interface. Therefore, we have selected the first, second, and other possible layers of the water slab, and we compared them with a segment that has the same thickness in the middle part of the confined system. We also compared these results with a similar segment in pure SPC/E water without confinement.

As can be seen from Fig. 7, the residence time of confined water molecules at the interface (green and purple lines) is more than the residence time of molecules in the bulk (dashed yellow and dashed-dotted black lines). This indicates that the strength of H-bonds in the first layer's hydrogen network is higher than that in areas closer to the bulk, and water molecules tend to stay at this layer for a longer period of time. This observation is in agreement with our earlier observations of the existence of a strong H-bond network in this layer.

To obtain more quantitative measures on the timescales associated with water exchange in the different layers near graphene and how it compares to the bulk, we found that they could be fit to a maximum of two exponential functions of the following form:

$$N_w(t) = n_1 e^{-t/\tau_1} + n_2 e^{-t/\tau_2} + n_p. \tag{5}$$

Here, n_p is the number of water molecules that permanently and continuously are in the selected region. We have summarized the data for the system with $L_z = 24.8$ Å in Table I.

As can be seen from Table I (and from Tables II, III, and IV in Appendix B), one needs two exponential terms to describe the behavior of residence time for the first and second layers. This can be attributed to two populations of water molecules, one that is involved in a stronger hydrogen-bond network and another that is more labile, as discussed in the previous section. As one moves from the interface to the bulk, there is a reduction in the residence time by about a factor of 4, which is consistent with the notion that the bulk region of water is characterized by weaker hydrogen bonds. It should also be stressed that the slow-down in the water dynamics is not so drastic in the sense that the graphene-water interface is still a very dynamic system on the 10s of picosecond timescale. Similar features have also been observed using *ab initio* molecular dynamics simulations of water near graphene by Chandra *et al.* [59].

To understand better how the translational motion of a water molecule changes near the graphene surface, we computed the translational diffusivity from the mean-square displacement of the oxygen atoms of the water as described by the following canonical equation:

$$D_s = \frac{1}{N} \sum_{n=1}^{N} \left[r_n^{\alpha}(t) - r_n^{\alpha}(0) \right]^2, \quad \alpha = x, y, \tag{6}$$

where r_n^{α} is the position of the nth particle, N is the number of particles, and t is time. The time interval of 50 ps was chosen in acquiring the slope of MSD versus time that gives the diffusion constant. For our analysis, we found that the linear regime could be fit between XX and YY picoseconds in order to extract the diffusion constant.

Overall, Fig. 8(a) shows that the lateral diffusivity is higher at the interface compared to the bulk. Although the water molecules have a larger residence time at the interface, they are not rigid and exhibit enhanced mobility. This result is also consistent with previous studies [40,60–65] simulating water near graphene surfaces. We propose that the higher diffusivity of water molecules under confinement is due the motion of the entire hydrogen bond network in the horizontal plane and not because of the movement of water molecules as single units. This collective movement of water molecules is due to the unfavorable energy that is needed for one single molecule to leave the hydrogen bond network, as one would need to break an enthalpically stabilized strong hydrogen bond interaction. Therefore, water molecules tend to keep their collective configuration as planar clusters at the interface during diffusion. The distance that water molecules in a cluster travel is more than the distance of a single water molecule motion in the

TABLE I. Residence time results for $L_z = 24.8$ Å distance between graphene sheets.

Estimated layers	τ_1 (ps)	τ_2 (ps)	n_1	n_2	n_p
First layer	18.44	1.18	450.61	23.88	∼0
Second layer	6.34	0.97	395.16	53.22	∼0
Third layer	4.41		401.35		∼0
Middle layer (close to bulk)	4.24		400.18		∼0
Pure SPC/E water	4.28		445.85		∼0

bulk. This causes the higher lateral diffusion constants for water molecules at the interfaces.

To understand the underlying mechanism associated with the enhanced lateral diffusion, we computed the time-averaged z component of fluctuation in the center of mass of the whole system, which is shown in Fig. 8(a) for different slab thicknesses. The center of mass of the system is removed from $\sigma^2_{z,\mathrm{com}}$. We found that the behavior of the variance for confined systems' center of mass along the z direction as a function of water slab thickness mirrors the behavior seen in the lateral diffusion. We note that the drastic decrease in $\sigma^2_{z,\mathrm{com}}$ for $L_z = 7.5$ Å is due to the extreme confinement for the single layer of water molecules in the slab to move along the z direction. We also point out that all the values of $\sigma^2_{z,\mathrm{com}}$ for all confined systems are about ten times less than $\sigma^2_{z,\mathrm{com}}$ for the bulk water without confinement, that is, 3.47×10^{-5} nm^2.

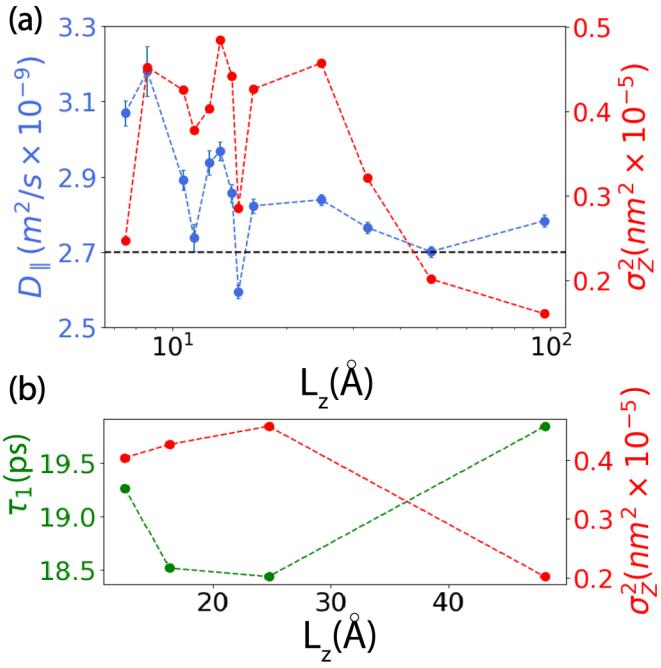

FIG. 8. (a) The lateral diffusivity (blue data) and variance in the z component of the center of mass (red data) of confined systems as a function of the thickness of the water slab. These two diagrams are shown together to compare the trends. This shows that the effect of commensurability and the hopping of water molecules between early layers of water are two factors determining the lateral diffusivity. The black dashed line shows the bulk value of the lateral diffusion constant for bulk water without confinement with graphene walls. (b) The behavior of residence time for the first layer and σ^2_z as defined in the main text. As can be seen from the diagram, τ_1 and $\sigma^2_{z,\mathrm{com}}$ have opposite trends, demonstrating that as the number of hopping increases (higher $\sigma^2_{z,\mathrm{com}}$), the residence time τ_1 decreases.

We can also relate the trends observed in the lateral diffusion to commensurability between the space required for the entire layer of water molecules to be embedded in the confined channel. The effect of commensurability has been observed in the study of other dynamical properties of confined water [26,66–90]. The oscillatory behavior of lateral diffusion in Fig. 8(a) for the channel widths below ∼30 Å is due to the commensurability for early water layers at the interface. This commensurability determines the hopping of water molecules among early surface layers for a slab with a fixed density. Some specific channel sizes, for example with a certain ratio of water molecules in the first and second layer as well as the rest of water, cause a minimum fluctuation in the z component in the center of mass of water. These channels are consistent with minimum interlayer water molecule hopping and, as discussed previously, minimum lateral diffusion. The same trend is true for other commensurabilities. This oscillatory behavior has been followed experimentally in atomic force microscopy (AFM) experiments [26,67,82,83] in which the solvation force varies with a period close to water molecule size, which is consistent with our computed period of oscillations. Indeed, the AFM results show that the dynamics of confined water depend significantly on the exact confining cavity size, which can determine the extent to which the water slab is commensurate with the water molecule thickness [84,91–94].

Here, we propose that when the number of water molecules hopping is larger, there will be a larger region for the clusters of water molecules in the early layers to move in the parallel direction to the graphene walls. After leaving a water molecule from a primary layer at the interface, adjacent water clusters in that planar layer fill the empty region. As a result, when the number of water molecules hopping among the early

TABLE II. Residence time results for $L_z = 12.4$ Å distance between graphene sheets.

Estimated layers	τ_1 (ps)	τ_2 (ps)	n_2	n_3	n_p
First layer	19.26	1.42	441.55	20.6	∼0
Second layer	8.42	1.05	360.80	41.82	∼0

TABLE III. Residence time results for $L_z = 16.4$ Å distance between graphene sheets.

Estimated layers	τ_1 (ps)	τ_2 (ps)	n_1	n_2	n_p
First layer	18.52	1.33	448.36	20.59	∼0
Second layer	7.30	1.00	398.05	51.61	∼0

layers is larger, the lateral diffusion increases. In contrast, when the number of water molecules hopping is small, the hydrogen bond networks are mostly compact next to each other and harder to move. This happens for the channel size of $L_z = 15.4$ Å, in which the fluctuations in the z component of the center of mass are minimum among confined water slabs with a thickness of less than ∼30 Å. Hence, both the hydrogen-bond networks and hopping between layers are deterministic factors to define the behavior of the lateral diffusion of water in confined channels. Furthermore, in Fig. 8(b) the residence time τ_1 and $\sigma^2_{z,\mathrm{com}}$ are compared. In agreement with previous discussions, these two quantities have opposite behavior, meaning that as the number of interlayer hopping at the interface is higher for the slab thickness L_z (higher $\sigma^2_{z,\mathrm{com}}$), the residence time of water molecules for the first layer is smaller. Therefore, interfacial water molecules in the slab with higher $\sigma^2_{z,\mathrm{com}}$ have a greater tendency to leave their initial layers to hop to another layer.

IV. CONCLUSIONS

In this work, we investigated the dielectric permittivity profile of water in slab and confined geometry between two parallel and neutral graphene layers. We considered the profile of $\varepsilon_\perp(z)$ as a function of height z in confined systems, and we found new relations between this quantity and the density of charges as well as fluctuations in the number of hydrogen and oxygen atoms per each atom separately as a function of height z in the channel. These findings led us to discover molecular scale differences in the types of motion and responses between hydrogen and oxygen atoms at the interface and in the bulk. Also, we followed the details in the changes of the dielectric response and water layer configurations, in which we can locate the dangling H-bonds in the region between the first and second layers of water.

Furthermore, we showed that the effective perpendicular dielectric constant decreases drastically when the distance between two graphene sheets decreases and reaches a value ∼1.4 in most extreme confined systems. The merging of the perpendicular dielectric constant with the bulk value of the SPC/E water model happens for thicknesses that are larger than our expectation of the water slab that should be in the bulk regions. The perpendicular dielectric constants in this work are in agreement with recent experimental data, in which the capacity model for determining the effective dielectric constant has been used among AFM measurements.

We show, by computing the residence time of water in different layers, that water molecules tend to remain in the first layer more than other parts of the channels, which is consistent with the existence of strong H-bonds in the hydration shell. Therefore, molecules in the second layer cannot make significant H-bonds with the first layer, creating dangling O-H bonds directed into the low-density region. The third layer and middle segment of water slabs have the same residence time in comparison to the pure SPC/E model. This demonstration is in agreement with a small population fluctuation per number of atoms for both hydrogen and oxygen at the interfaces.

Finally, we also determined the lateral self-diffusion constant of water under confinement, and we showed that for almost all channel thicknesses it is higher than the bulk value of the water. Therefore, in spite of the confinements, water molecules can diffuse in collective motions at the interface, causing higher values of lateral diffusivity. The key factor in determining the lateral diffusivity in confined structures for a fixed density is the number of water molecules hopping among the layers at the interface. The residence time and the fluctuation in the center of mass of water as a function of slab thickness have anticorrelated behavior, in agreement with the number of water molecules hopping for the interface layers. Finally, we believe that the insights into the behavior of water at the interface presented here can be followed in different systems among various disciplines, such as physics, geophysics, surface science, chemistry, and molecular biology.

ACKNOWLEDGMENTS

I.A. thanks Mehdi Hassanpour for helpful discussion in simulations of this work. A.H. and I.A. thank Muhammad Nawaz Qaisrani for the helpful conversation. The authors also acknowledge the HPC center of Sharif University of Technology.

APPENDIX A: REVIEW OF LINEAR-RESPONSE THEORY OF THE DIELECTRIC CONSTANT IN CONFINED SYSTEMS

Here, we review the theory of linear response and fluctuation-dissipation for the dielectric function for slab

TABLE IV. Residence time results for $L_z = 42.8$ Å distance between graphene sheets.

Estimated layers	τ_1 (ps)	τ_2 (ps)	n_1	n_2	n_p
First layer	19.84	1.28	461.9	18.38	∼0
Second layer	7.38	1.02	407.68	52.71	∼0
Third layer	4.74		421.50		∼0
Middle layer (close to bulk)	4.27		423.13		∼0

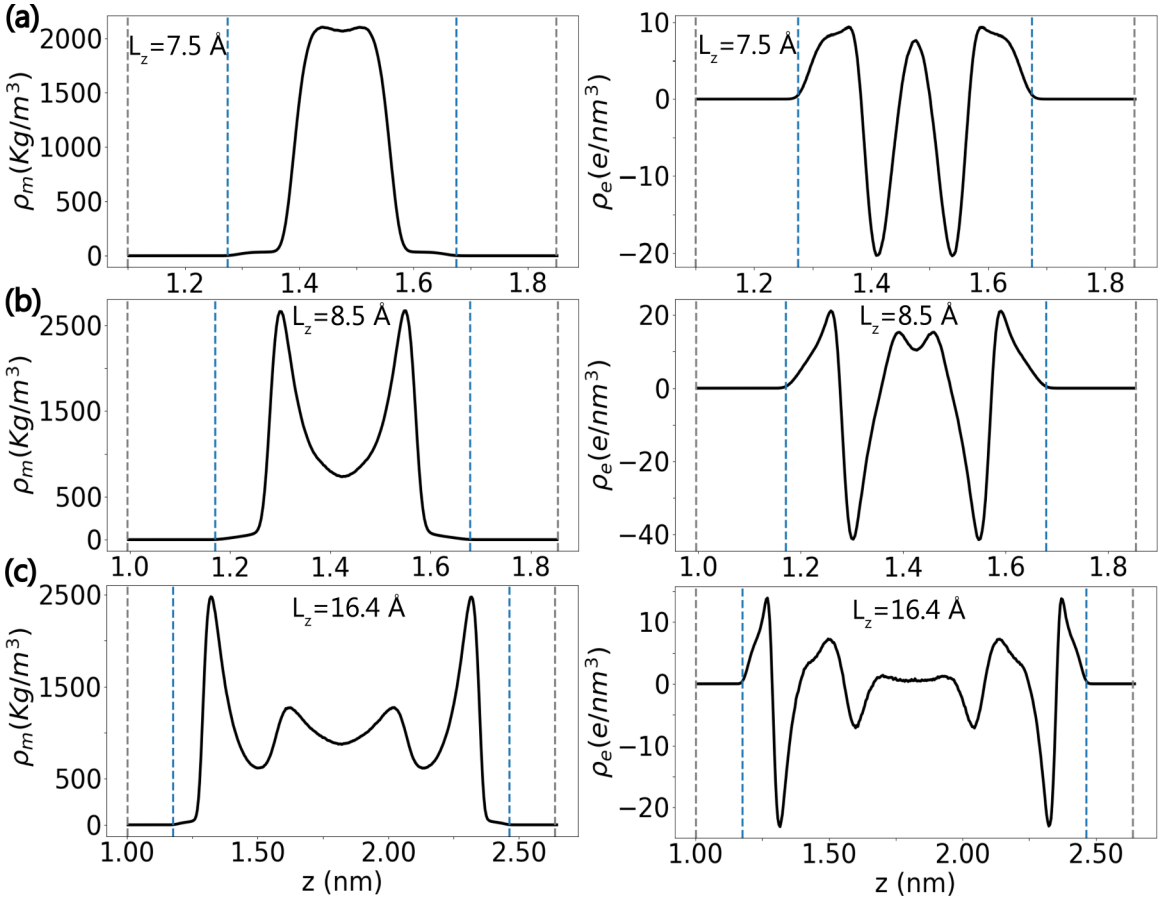

FIG. 9. Molecular (left) and charge (right) densities of confined water in channels with different heights. Dashed lines in gray and blue indicate the position of graphene and water, respectively. The particle density indicates the layered structure of water under confinement, and it also indicates a dense layer in the first layer of water closest to graphene surfaces. Extreme reduction in the density of particles after the first maximum on both sides of the diagrams shows the low-density region with a thickness of ∼2 Å between the first and the second layers of water. The diagrams for the density of charges reveal more tendency of hydrogen atoms to be near graphene sheets. This demonstrates that the total charges in the low-density region between the first and the second layer of water are positive, following the presence of dangling O-H bonds in these regions. The water slabs in the figure are (a) $L_z = 7.5$ Å, (b) $L_z = 8.5$ Å, and (c) $L_z = 16.4$ Å.

geometries such as our system of study [25,34,35,39,40]. The change in dielectric displacement field is related linearly to the change of electric field in the linear-response regime via the equation

$$\Delta \boldsymbol{D} = \varepsilon_0 \int \Delta \boldsymbol{E}(\boldsymbol{r}') \cdot \varepsilon_{\rm nl}(\boldsymbol{r}, \boldsymbol{r}') d\boldsymbol{r}', \tag{A1}$$

where ε_0 is vacuum permittivity, $E(r')$ is a local electric field, and $\varepsilon_{\rm nl}(\boldsymbol{r}, \boldsymbol{r}')$ is a nonlocal dielectric tensor. A constant electric field in a homogeneous system results in a local response function as a product of the permittivity tensor. Change in the electric field is given by

$$\Delta \boldsymbol{D} = \varepsilon_0 \varepsilon(\boldsymbol{r}) \cdot \Delta \boldsymbol{E}, \tag{A2}$$

where $\varepsilon(\boldsymbol{r}) = \int \varepsilon_{\rm nl}(\boldsymbol{r}, \boldsymbol{r}') d\boldsymbol{r}'$, and using a local assumption then we have $\varepsilon_{\rm nl}(\boldsymbol{r}, \boldsymbol{r}') = \delta(\boldsymbol{r} - \boldsymbol{r}')\varepsilon(\boldsymbol{r})$. The inverse of the dielectric response function is defined similarly,

$$\Delta \boldsymbol{E} = \varepsilon_0^{-1} \int \Delta \boldsymbol{D}(\boldsymbol{r}') \cdot \varepsilon_{\rm nl}^{-1}(\boldsymbol{r}, \boldsymbol{r}') d\boldsymbol{r}', \tag{A3}$$

where $\varepsilon_{\rm nl}^{-1}(\boldsymbol{r}, \boldsymbol{r}')$ is the inverse of $\varepsilon_{\rm nl}(\boldsymbol{r}, \boldsymbol{r}')$ defined by $\delta(\boldsymbol{r} - \boldsymbol{r}') = \int \varepsilon_{\rm nl}(\boldsymbol{r}, \boldsymbol{r}')\varepsilon_{\rm nl}^{-1}(\boldsymbol{r}', \boldsymbol{r}'') d\boldsymbol{r}'$, and when the displacement of the field is constant, similar to the above discussion, the inverse dielectric response function is local and results in [25,34,35,39,40]

$$\Delta \boldsymbol{E} = \varepsilon_0^{-1} \varepsilon^{-1}(\boldsymbol{r}) \cdot \Delta \boldsymbol{D}, \tag{A4}$$

in which $\varepsilon^{-1}(\boldsymbol{r})$ is the inverse of the dielectric tensor. For the perpendicular component of the electric field and the dielectric displacement field, we obtain the following similar equations [25,34,35,39,40]:

$$\Delta E_\perp(z) = \varepsilon_0^{-1} \varepsilon_\perp^{-1}(z) \Delta D_\perp. \tag{A5}$$

The electric field is separated into the displacement field, $\boldsymbol{D}(\boldsymbol{r})$, for monopole terms in the integral of the electric field and the polarization $\boldsymbol{m}(\boldsymbol{r})$ for all higher multimoments of the electric field, yielding $\varepsilon_0 \boldsymbol{E}(\boldsymbol{r}) = \boldsymbol{D}(\boldsymbol{r}) - \boldsymbol{m}(\boldsymbol{r})$ as given by [35]

$$\varepsilon_0 \boldsymbol{E}(\boldsymbol{r}) = \frac{1}{4\pi} \int \rho(\boldsymbol{r}') \frac{\boldsymbol{r} - \boldsymbol{r}'}{|\boldsymbol{r} - \boldsymbol{r}'|^3} d\boldsymbol{r}', \tag{A6}$$

$$\varepsilon_0 \boldsymbol{E} = \boldsymbol{D} - \boldsymbol{m}, \tag{A7}$$

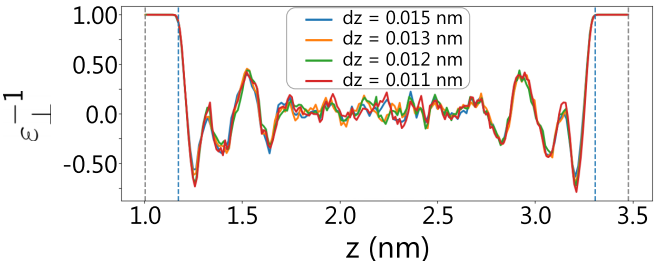

FIG. 10. Four different choices of dz in order to show that the changes in the perpendicular component of the dielectric constant are independent of bin size dz.

where $\rho(\boldsymbol{r})$ is the total charge density. The definition of the total polarization $\boldsymbol{M}$ is

$$\boldsymbol{M} = \int_V \boldsymbol{m}(\boldsymbol{r}) d\boldsymbol{r}. \tag{A8}$$

The integral is over the volume of V. Through fluctuation-dissipation theory, in the presence of an external homogeneous electric field $\boldsymbol{F}$, the change in the polarization is defined by [35]

$$\Delta \boldsymbol{m}(\boldsymbol{r}) = \langle \boldsymbol{m}(\boldsymbol{r}) \rangle_{\boldsymbol{F}} - \langle \boldsymbol{m}(\boldsymbol{r}) \rangle_0. \tag{A9}$$

In the form of the ensemble average,

$$\Delta \boldsymbol{m}(\boldsymbol{r}) = \frac{\int (\boldsymbol{m} - \langle \boldsymbol{m} \rangle_0) \exp[-\beta(U - \boldsymbol{M} \cdot \boldsymbol{F})] d\mathcal{P}}{\int \exp[-\beta(U - \boldsymbol{M} \cdot \boldsymbol{F})] d\mathcal{P}}, \tag{A10}$$

where $d\mathcal{P} = \prod_i d\boldsymbol{r}_i d\boldsymbol{q}_i$ denotes the integration on the phase region over all directions and positions, indices 0 and $\boldsymbol{F}$ denote the absence and presence of an external field, respectively. This equation can be linearized for a small magnitude of $\boldsymbol{F}$ (in the linear-response regime) to be [34]

$$\Delta \boldsymbol{m}(\boldsymbol{r}) \approx [\langle \boldsymbol{m}(\boldsymbol{r}) \boldsymbol{M} \rangle_0 - \langle \boldsymbol{m}(\boldsymbol{r}) \rangle_0 \langle \boldsymbol{M} \rangle_0] \cdot \boldsymbol{F}. \tag{A11}$$

In the current case study of slab geometry, ensemble-averaged quantities depend only on the z component of the spatial region. In the perpendicular direction, the vanishing of the average monopole density condition as $\nabla \cdot \boldsymbol{D}(z) = \boldsymbol{0}$ and the boundary condition of $\Delta D_\perp(z) = D_\perp$ indicates a constant displacement field. By applying Eqs. (A5) and (A7), we obtain the following equation:

$$\varepsilon_\perp^{-1}(z) = 1 - \frac{\Delta m_\perp(z)}{D_\perp}. \tag{A12}$$

We note that the field $F_\perp$ is equal to $D_\perp/\varepsilon_0$. Using Eqs. (A11) and (A12) with the definitions $\Delta m_\perp(z) = \langle m_\perp(z) M_\perp \rangle - \langle m_\perp(z) \rangle \langle M_\perp \rangle$ and $C_\perp = L_x L_y \int_{L_z} \Delta m_\perp(z) dz$, we obtain [25]

$$\varepsilon_\perp^{-1}(z) = 1 - \frac{\Delta m_\perp(z)}{\varepsilon_0 k_B T + C_\perp / V}, \tag{A13}$$

where L_x and L_y are the length of the system in the x and y directions. We can calculate the polarization as an integral of the charge distribution $\rho(\boldsymbol{r})$ over volume. Therefore, the $m_\perp(z)$ could be written as [40]

$$m_\perp(z) = -\int_0^z \rho(z') dz', \tag{A14}$$

where $\rho(z')dz'$ is the density of charges at height z'.

APPENDIX B: COMPLEMENTARY DATA

In this Appendix, we show the layered structure of water in confined slab geometry via the density of particles and charges as a function of z in the direction perpendicular to the graphene surfaces (Fig. 9).

Here, we show the dielectric profile of water in the perpendicular direction for different values of dz in order to show that the changes in the perpendicular dielectric component are independent of the dz value. We can see from the diagram in Fig. 10 that the trends of dielectric permittivity in the z direction are the same for four different choices of dz.

In Tables II, III, and IV, we present more data on the fitting of residence time and Eq. (5) for different slab thicknesses.

[1] D. Chandler, Interfaces and the driving force of hydrophobic assembly, Nature (London) **437**, 640 (2005).
[2] P. Ball, Water as an active constituent in cell biology, Chem. Rev. **108**, 74 (2008).
[3] F. Franks, *Water: A Matrix of Life* (Royal Society of Chemistry, London, 2007).
[4] G. Hummer, J. C. Rasaiah, and J. P. Noworyta, Water conduction through the hydrophobic channel of a carbon nanotube, Nature (London) **414**, 188 (2001).
[5] E. Breynaert, M. Houlleberghs, S. Radhakrishnan, G. Grübel, F. Taulelle, and J. A. Martens, Water as a tuneable solvent: A perspective, Chem. Soc. Rev. **49**, 2557 (2020).
[6] J. Beau and W. Webber, Studies of nano-structured liquids in confined geometry and at surfaces, Prog. Nucl. Magn. Res. Spectrosc. **56**, 78 (2010).
[7] J.-P. Korb, M. W. Hodges, Th. Gobron, and R. G. Bryant, Anomalous surface diffusion of water compared to aprotic liquids in nanopores, Phys. Rev. E **60**, 3097 (1999).
[8] F. Mallamace, C. Corsaro, P. Baglioni, E. Fratini, and S.-H. Chen, The dynamical crossover phenomenon in bulk water, confined water and protein hydration water, J. Phys.: Condens. Matter **24**, 064103 (2012).
[9] G. Algara-Siller, O. Lehtinen, F. C. Wang, R. R. Nair, U. Kaiser, H. A. Wu, A. K. Geim, and I. V. Grigorieva, Square ice in graphene nanocapillaries, Nature (London) **519**, 443 (2015).
[10] V. V. Chaban, V. V. Prezhdo, and O. V. Prezhdo, Confinement by carbon nanotubes drastically alters the boiling and critical behavior of water droplets, ACS Nano **6**, 2766 (2012).
[11] E. Secchi, S. Marbach, A. Niguès, D. Stein, A. Siria, and L. Bocquet, Massive radius-dependent flow slippage in carbon nanotubes, Nature (London) **537**, 210 (2016).
[12] J.-M. Zanotti, M.-C. Bellissent-Funel, and S.-H. Chen, Relaxational dynamics of supercooled water in porous glass, Phys. Rev. E **59**, 3084 (1999).
[13] H. Jansson and J. Swenson, Dynamics of water in molecular sieves by dielectric spectroscopy, Eur. Phys. J. E **12**, 51 (2003).

[14] J. J. Gilijamse, A. J. Lock, and H. J. Bakker, Dynamics of confined water molecules, Proc. Natl. Acad. Sci. (USA) **102**, 3202 (2005).

[15] L. Xu and V. Molinero, Is there a liquid–liquid transition in confined water? J. Phys. Chem. B **115**, 14210 (2011).

[16] M. F. Harrach and B. Drossel, Structure and dynamics of TIP3P, TIP4P, and TIP5P water near smooth and atomistic walls of different hydroaffinity, J. Chem. Phys. **140**, 174501 (2014).

[17] A. Faraone, L. Liu, C.-Y. Mou, C.-W. Yen, and S.-H. Chen, Fragile-to-strong liquid transition in deeply supercooled confined water, J. Chem. Phys. **121**, 10843 (2004).

[18] J. C. Rasaiah, S. Garde, and G. Hummer, Water in nonpolar confinement: From nanotubes to proteins and beyond, Annu. Rev. Phys. Chem. **59**, 713 (2008).

[19] S. Senapati and A. Chandra, Dielectric constant of water confined in a nanocavity, J. Phys. Chem. B **105**, 5106 (2001).

[20] A. Sugahara, Y. Ando, S. Kajiyama, K. Yazawa, K. Gotoh, M. Otani, M. Okubo, and A. Yamada, Negative dielectric constant of water confined in nanosheets, Nat. Commun. **10**, 850 (2019).

[21] G. Liu, W. Jin, and N. Xu, Graphene-based membranes, Chem. Soc. Rev. **44**, 5016 (2015).

[22] S. A. Miller, V. Y. Young, and C. R. Martin, Electroosmotic flow in template-prepared carbon nanotube membranes, J. Am. Chem. Soc. **123**, 12335 (2001).

[23] C. Dellago, M. M. Naor, and G. Hummer, Proton Transport Through Water-Filled Carbon Nanotubes, Phys. Rev. Lett. **90**, 105902 (2003).

[24] K.-D. Kreuer, S. J. Paddison, E. Spohr, and M. Schuster, Transport in proton conductors for fuel-cell applications: Simulations, elementary reactions, and phenomenology, Chem. Rev. **104**, 4637 (2004).

[25] V. Ballenegger and J.-P. Hansen, Dielectric permittivity profiles of confined polar fluids, J. Chem. Phys. **122**, 114711 (2005).

[26] A. Verdaguer, G. M. Sacha, H. Bluhm, and M. Salmeron, Molecular structure of water at interfaces: Wetting at the nanometer scale, Chem. Rev. **106**, 1478 (2006).

[27] P. K. Yuet and D. Blankschtein, Molecular dynamics simulation study of water surfaces: Comparison of flexible water models, J. Phys. Chem. B **114**, 13786 (2010).

[28] H. Li and X. C. Zeng, Wetting and interfacial properties of water nanodroplets in contact with graphene and monolayer boron–nitride sheets, ACS Nano **6**, 2401 (2012).

[29] M. Sharma, R. Resta, and R. Car, Intermolecular Dynamical Charge Fluctuations in Water: A Signature of the H-Bond Network, Phys. Rev. Lett. **95**, 187401 (2005).

[30] T. Werder, J. H. Walther, R. L. Jaffe, T. Halicioglu, and P. Koumoutsakos, On the water-carbon interaction for use in molecular dynamics simulations of graphite and carbon nanotubes, J. Phys. Chem. B **107**, 1345 (2003).

[31] S. Ruiz-Barragan, D. Muñoz-Santiburcio, S. Körning, and D. Marx, Quantifying anisotropic dielectric response properties of nanoconfined water within graphene slit pores, Phys. Chem. Chem. Phys. **22**, 10833 (2020).

[32] C. Schaaf and S. Gekle, Spatially resolved dielectric constant of confined water and its connection to the non-local nature of bulk water, J. Chem. Phys. **145**, 084901 (2016).

[33] P. A. Bopp, A. A. Kornyshev, and G. Sutmann, Frequency and wave-vector dependent dielectric function of water: Collective modes and relaxation spectra, J. Chem. Phys. **109**, 1939 (1998).

[34] D. J. Bonthuis, S. Gekle, and R. R. Netz, Profile of the static permittivity tensor of water at interfaces: Consequences for capacitance, hydration interaction and ion adsorption, Langmuir **28**, 7679 (2012).

[35] D. J. Bonthuis, S. Gekle, and R. R. Netz, Dielectric Profile of Interfacial Water and its Effect on Double-Layer Capacitance, Phys. Rev. Lett. **107**, 166102 (2011).

[36] S. Varghese, S. K. Kannam, J. S. Hansen, and S. P. Sathian, Effect of hydrogen bonds on the dielectric properties of interfacial water, Langmuir **35**, 8159 (2019).

[37] H. Jalali, H. Ghorbanfekr, I. Hamid, M. Neek-Amal, R. Rashidi, and F. M. Peeters, Out-of-plane permittivity of confined water, Phys. Rev. E **102**, 022803 (2020).

[38] C. Calero and G. Franzese, Water under extreme confinement in graphene: Oscillatory dynamics, structure, and hydration pressure explained as a function of the confinement width, J. Mol. Liq. **317**, 114027 (2020).

[39] A. A. Kornyshev, W. Schmickler, and M. A. Vorotyntsev, Nonlocal electrostatic approach to the problem of a double layer at a metal-electrolyte interface, Phys. Rev. B **25**, 5244 (1982).

[40] A. Schlaich, E. W. Knapp, and R. R. Netz, Water Dielectric Effects in Planar Confinement, Phys. Rev. Lett. **117**, 048001 (2016).

[41] J. B. Hasted, *Aqueous Dielectrics* (Chapman and Hall, London, 1973).

[42] L. Fumagalli, A. Esfandiar, R. Fabregas, S. Hu, P. Ares, A. Janardanan, Q. Yang, B. Radha, T. Taniguchi, K. Watanabe *et al.*, Anomalously low dielectric constant of confined water, Science **360**, 1339 (2018).

[43] D. J. Bonthuis and R. R. Netz, Unraveling the combined effects of dielectric and viscosity profiles on surface capacitance, electro-osmotic mobility, and electric surface conductivity, Langmuir **28**, 16049 (2012).

[44] D. Konatham, J. Yu, Tuan A. Ho, and A. Striolo, Simulation insights for graphene-based water desalination membranes, Langmuir **29**, 11884 (2013).

[45] H. J. C. Berendsen, J. R. Grigera, and T. P. Straatsma, The missing term in effective pair potentials, J. Phys. Chem. **91**, 6269 (1987).

[46] D. V. Der Spoel, E. Lindahl, B. Hess, G. Groenhof, A. E. Mark, and H. J. C. Berendsen, Gromacs: Fast, Flexible, and Free, J. Comput. Chem. **26**, 1701 (2005).

[47] S. Nosé, A unified formulation of the constant temperature molecular dynamics methods, J. Chem. Phys. **81**, 511 (1984).

[48] W. G. Hoover, Canonical dynamics: Equilibrium phase-space distributions, Phys. Rev. A **31**, 1695 (1985).

[49] U. Essmann, L. Perera, M. L. Berkowitz, T. Darden, H. Lee, and L. G. Pedersen, A smooth particle mesh ewald method, J. Chem. Phys. **103**, 8577 (1995).

[50] M. Sharma, R. Resta, and R. Car, Dipolar Correlations and the Dielectric Permittivity of Water, Phys. Rev. Lett. **98**, 247401 (2007).

[51] M. Neumann, Dipole moment fluctuation formulas in computer simulations of polar systems, Mol. Phys. **50**, 841 (1983).

[52] C. Zhang, F. Gygi, and G. Galli, Strongly anisotropic dielectric relaxation of water at the nanoscale, J. Phys. Chem. Lett. **4**, 2477 (2013).

[53] J. Rafiee, X. Mi, H. Gullapalli, A. V. Thomas, F. Yavari, Y. Shi, P. M. Ajayan, and N. A. Koratkar, Wetting transparency of graphene, Nat. Mater. **11**, 217 (2012).

[54] A. Luzar and D. Chandler, Hydrogen-bond kinetics in liquid water, Nature (London) **379**, 55 (1996).

[55] A. Kayal and A. Chandra, Water in confinement between nanowalls: Results for hexagonal boron nitride versus graphene sheets from *ab initio* molecular dynamics, J. Phys. Chem. C **123**, 6130 (2019).

[56] D. M. Huang, C. Cottin-Bizonne, C. Ybert, and L. Bocquet, Aqueous electrolytes near hydrophobic surfaces: Dynamic effects of ion specificity and hydrodynamic slip, Langmuir **24**, 1442 (2008).

[57] M. Mohammadi-Arzanagh, S. Mahdisoltani, R. Podgornik, and A. Naji, Hydrodynamic stress correlations in fluid films driven by stochastic surface forcing, Phys. Rev. Fluids **3**, 064201 (2018).

[58] C.-J. Shih, S. Lin, M. S. Strano, and D. Blankschtein, Understanding the stabilization of liquid-phase-exfoliated graphene in polar solvents: Molecular dynamics simulations and kinetic theory of colloid aggregation, J. Am. Chem. Soc. **132**, 14638 (2010).

[59] D. V. der Spoel, P. J. V. Maaren, and H. J. C. Berendsen, A systematic study of water models for molecular simulation: Derivation of water models optimized for use with a reaction field, J. Chem. Phys. **108**, 10220 (1998).

[60] G. Cicero, J. C. Grossman, E. Schwegler, F. Gygi, and G. Galli, Water confined in nanotubes and between graphene sheets: A first principle study, J. Am. Chem. Soc. **130**, 1871 (2008).

[61] K. Koga, G. T. Gao, H. Tanaka, and X. C. Zeng, Formation of ordered ice nanotubes inside carbon nanotubes, Nature (London) **412**, 802 (2001).

[62] Q. Lu and J. E. Straub, Freezing transitions of nanoconfined coarse-grained water show subtle dependence on confining environment, J. Phys. Chem. B **120**, 2517 (2016).

[63] M. Neek-Amal, F. M. Peeters, I. V. Grigorieva, and A. K. Geim, Commensurability effects in viscosity of nanoconfined water, ACS Nano **10**, 3685 (2016).

[64] S. Buyukdagli and R. Blossey, Dipolar correlations in structured solvents under nanoconfinement, J. Chem. Phys. **140**, 234903 (2014).

[65] Y. Wu, H. L. Tepper, and G. A. Voth, Flexible simple point-charge water model with improved liquid-state properties, J. Chem. Phys. **124**, 024503 (2006).

[66] Z. Qian and G. Wei, Electric-field-induced phase transition of confined water nanofilms between two graphene sheets, J. Phys. Chem. A **118**, 8922 (2014).

[67] S. Parez, M. Predota, and M. Machesky, Dielectric properties of water at rutile and graphite surfaces: Effect of molecular structure, J. Phys. Chem. C **118**, 4818 (2014).

[68] D. Cohen-Tanugi and J. C. Grossman, Water desalination across nanoporous graphene, Nano Lett. **12**, 3602 (2012).

[69] S. Han, M. Y. Choi, P. Kumar, and H. E. Stanley, Phase transitions in confined water nanofilms, Nat. Phys. **6**, 685 (2010).

[70] U. Fano, Ionization yield of radiations. ii. The fluctuations of the number of ions, Phys. Rev. **72**, 26 (1947).

[71] P. Kumar, S. V. Buldyrev, F. W. Starr, N. Giovambattista, and H. E. Stanley, Thermodynamics, structure, and dynamics of water confined between hydrophobic plates, Phys. Rev. E **72**, 051503 (2005).

[72] A. Amjadi, R. Shirsavar, N. H. Radja, and M. R. Ejtehadi, A liquid film motor, Microfluid. Nanofluid. **6**, 711 (2009).

[73] A. I. Kolesnikov, J.-M. Zanotti, C.-K. Loong, P. Thiyagarajan, A. P. Moravsky, R. O. Loutfy, and C. J. Burnham, Anomalously Soft Dynamics of Water in a Nanotube: A Revelation of Nanoscale Confinement, Phys. Rev. Lett. **93**, 035503 (2004).

[74] A. A. Hassanali and S. J. Singer, Model for the water-amorphous silica interface: The undissociated surface, J. Phys. Chem. B **111**, 11181 (2007).

[75] H. Zhang, A. A. Hassanali, Y. K. Shin, C. Knight, and S. J. Singer, The water–amorphous silica interface: Analysis of the stern layer and surface conduction, J. Chem. Phys. **134**, 024705 (2011).

[76] A. A. Hassanali, H. Zhang, C. Knight, Y. K. Shin, and S. J. Singer, The dissociated amorphous silica surface: Model development and evaluation, J. Chem. Theory Comput. **6**, 3456 (2010).

[77] M. Neumann and O. Steinhauser, On the calculation of the frequency-dependent dielectric constant in computer simulations, Chem. Phys. Lett. **102**, 508 (1983).

[78] F. Pizzitutti, M. Marchi, F. Sterpone, and P. J. Rossky, How protein surfaces induce anomalous dynamics of hydration water, J. Phys. Chem. B **111**, 7584 (2007).

[79] M. N. Qaisrani, L. Grisanti, R. Gebauer, and A. Hassanali, Structural and dynamical heterogeneities at glutamine–water interfaces, Phys. Chem. Chem. Phys. **21**, 16083 (2019).

[80] M. K. Rana and A. Chandra, Ab initio and classical molecular dynamics studies of the structural and dynamical behavior of water near a hydrophobic graphene sheet, J. Chem. Phys. **138**, 204702 (2013).

[81] S. De Luca, S. K. Kannam, B. D. Todd, F. Frascoli, J. S. Hansen, and P. J. Daivis, Effects of confinement on the dielectric response of water extends up to mesoscale dimensions, Langmuir **32**, 4765 (2016).

[82] J. Gao, W. D. Luedtke, and U. Landman, Origins of solvation forces in confined films, J. Phys. Chem. B **101**, 4013 (1997).

[83] J. P. Cleveland, T. E. Schäffer, and P. K. Hansma, Probing oscillatory hydration potentials using thermal-mechanical noise in an atomic-force microscope, Phys. Rev. B **52**, R8692 (1995).

[84] S. Jeffery, P. M. Hoffmann, J. B. Pethica, C. Ramanujan, H. Ö. Özer, and A. Oral, Direct measurement of molecular stiffness and damping in confined water layers, Phys. Rev. B **70**, 054114 (2004).

[85] A. Keerthi, A. K. Geim, A. Janardanan, A. P. Rooney, A. Esfandiar, S. Hu, S. A. Dar, I. V. Grigorieva, S. J. Haigh, F. C. Wang *et al.*, Ballistic molecular transport through two-dimensional channels, Nature (London) **558**, 420 (2018).

[86] P. L. Silvestrelli and M. Parrinello, Water Molecule Dipole in the Gas and in the Liquid Phase, Phys. Rev. Lett. **82**, 3308 (1999).

[87] M. Chen, H.-Y. Ko, R. C. Remsing, M. F. C. Andrade, B. Santra, Z. Sun, A. Selloni, R. Car, M. L. Klein, J. P. Perdew *et al.*, Ab initio theory and modeling of water, Proc. Natl. Acad. Sci. (USA) **114**, 10846 (2017).

[88] P. Hirunsit and P. B. Balbuena, Effects of confinement on water structure and dynamics: A molecular simulation study, J. Phys. Chem. C **111**, 1709 (2007).

[89] H. Ghorbanfekr, J. Behler, and F. M. Peeters, Insights into water permeation through HBN nanocapillaries by *ab initio* machine learning molecular dynamics simulations, J. Phys. Chem. Lett. **111**, 7363 (2020).

[90] P. Mark and L. Nilsson, Structure and dynamics of the TIP3P, SPC, and SPC/E water models at 298 k, J. Phys. Chem. A **105**, 9954 (2001).

[91] K. Gopinadhan, S. Hu, A. Esfandiar, M. Lozada-Hidalgo, F. C. Wang, Q. Yang, A. V. Tyurnina, A. Keerthi, B. Radha, and A. K. Geim, Complete steric exclusion of ions and proton transport through confined monolayer water, Science **363**, 145 (2019).

[92] N. Dwivedi, T. Patra, J.-B. Lee, R. J. Yeo, S. Srinivasan, T. Dutta, K. Sasikumar, C. Dhand, S. Tripathy, M. S. M. Saifullah *et al.*, Slippery and wear-resistant surfaces enabled by interface engineered graphene, Nano Lett. **20**, 905 (2019).

[93] S. Ruiz-Barragan, D. M. Santiburcio, and D. Marx, Nanoconfined water within graphene slit pores adopts distinct confinement-dependent regimes, J. Phys. Chem. Lett. **10**, 329 (2018).

[94] A. Esfandiar, B. Radha, F. C. Wang, Q. Yang, S. Hu, S. Garaj, R. R. Nair, A. K. Geim, and K. Gopinadhan, Size effect in ion transport through angstrom-scale slits, Science **358**, 511 (2017).